

2717511 High-resolution seismic velocity structure of the shallow Porcupine Basin from travelttime tomography and waveform inversion of long-streamer data

M. Prada ^{1,2}, F. Lavoué ^{1,2}, B. O'Reilly ^{1,2}, S. Lebedev ^{1,2}, Y. Yuan ³, C. Gras ⁴

¹ Irish Centre for Research in Applied Geosciences (iCRAG)

² Dublin Institute for Advanced Studies, Geophysics Section, 5 Merrion square, Dublin, Ireland

³ Princeton University, Department of Geosciences, Princeton (NJ), USA

⁴ Barcelona Center for Subsurface Imaging, Marine Science Institute, CSIC, Barcelona, Spain

The Porcupine Basin is a failed rift located in the North Atlantic margin southwest of Ireland. This triangular-shaped basin was formed after several rifting and subsidence phases during Late Paleozoic Mesozoic and Cenozoic, with the most pronounced rift phase occurring in Late Jurassic–Early Cretaceous times. From the perspective of hydrocarbon exploration, the Porcupine Basin is one of the most attractive regions of the North Atlantic with potential hydrocarbon systems within the post-rift stratigraphic sequence (i.e. Cretaceous and Tertiary sediments), in addition to potential in the pre- and syn-rift sequences. Seismic reflection lines reveal gas chimneys and seeps potentially associated with buried carbonate mounds and indicating the presence of deeper hydrocarbon systems within the post-rift section of the basin. Yet, these areas are not thoroughly explored and little is known regarding properties of rocks, such as porosity and fluid content, both critical for reservoir characterization. Here, we combine travelttime tomography and full waveform inversion of 10 km-long streamer data to obtain 2D seismic velocity images of the Cretaceous and Tertiary sequences of the Porcupine basin with unprecedented resolution. First, we apply travelttime tomography of automatically selected first arrivals from streamer field data. For those lines acquired in deep (~ 1000 m) water, we use a downward continuation method to redatum seismic shot gathers to the seafloor, which allows the identification of P-wave arrival times previously masked by the reflection at the seafloor. The resultant tomographic models resolve low-wavenumber P-wave velocity structures of the shallow Porcupine Basin providing a satisfactory starting model for the waveform inversion. This second step makes use of recent formulations of the misfit function between observed and synthetic waveforms, which enhance the robustness of the inversion, and aims for finer resolution than travelttime tomography. The waveform inversion of streamer data is expected to provide sub-wavelength images of seismic velocities and in the long-term of density and/or anisotropy. All these parameters can be used to derive physical properties of rocks and assess the potential of the post-rift sequence to host petroleum reservoirs.

1 Introduction

During the Mesozoic, the opening of the North Atlantic Ocean triggered a large pulse of extension that resulted in the formation of large sedimentary basins like the Porcupine Basin, offshore SW Ireland (Fig. 1a). Plate kinematic models suggest that the Porcupine Basin was formed at the same stage than the Jeanne d'Arc and Orphan Basin, located now at the conjugate margin of Newfoundland, offshore Canada (e.g. [Sirvastava and Verhoef, 1992](#)). The Canadian Atlantic margin is considered an important petroleum province with successful discoveries and potential for hosting new giant fields within these Mesozoic basins ([Enachescu and Hogg, 2005](#)), which makes the Porcupine Basin an ideal candidate for hosting similar petroleum systems.

Interestingly, basin modelling derived from seismic reflection and well data suggest the presence of working petroleum systems within the post-rift stratigraphic sequence of the Porcupine ([Naeth et al., 2005](#)). The post-rift sequence in the Porcupine contains Cretaceous and Cenozoic sediments deposited during several episodes of thermal subsidence ([Shannon et al., 1993](#)). Thermal subsidence has also contributed to the formation of normal faulting within the post-rift and the reactivation of former syn-rift basin-bounding faults ([Worthington and Walsh, 2016](#)). Normal faulting within the post-rift section is thought to be key in controlling the migration of fluids/hydrocarbons to the surface, as well as in controlling the initiation of carbonate seamounts in the Porcupine Basin ([Hovland et al., 1993](#)). However, little is known regarding the petrophysical properties associated to the shallow post-rift sequence such as porosity and fluid content, both critical for reservoir characterization. The only reliable source of information regarding these parameters come from the limited amount of wells drilled in the basin. However, boreholes are mostly restricted to the northern section of the basin, and they only provide insights from discrete and localized points of the sedimentary basin. An indirect way of estimating petrophysical properties over broad sections of the subsurface would be to infer them from seismic properties (e.g. V_p , V_s , density, attenuation, anisotropy) from tomographic images using petrophysical relationships (e.g. [Erickson and Jarrard, 1998](#)).

Over the last decade, a large number of studies have proven that combining traveltimes tomography and full waveform inversion (FWI) of long-streamer data can provide quantitative images of subsurface seismic properties with unprecedented detail (e.g. [Hicks and Pratt, 2001](#); [Sirgue et al., 2010](#); [Delescluse et al., 2011](#)). Ray-based traveltimes tomography provides smoother tomographic images, but is also much more robust, than FWI. Indeed, one of the pitfalls of FWI based on gradient search optimization methods is that local minima may lead to incorrect solutions, unless the data contains long-offset reflected and refracted arrivals, the inversion begins at the lowest possible frequency, and a good starting velocity model is used (e.g. [Sirgue and Pratt, 2004](#); [Virieux and Operto, 2009](#)). This latter aspect is commonly overcome by using smooth velocity models obtained from first arrival traveltimes tomography (FATT) as starting models for FWI (e.g. [Hicks and Pratt, 2001](#); [Delescluse et al., 2011](#)).

Here we present preliminary results of a new study that interrogates the petrophysical structure of the shallow (mostly post-rift) Porcupine Basin from FATT and FWI of 10-km-long streamer data. We apply FATT to obtain a first tomographic image of the P-wave seismic velocity (V_p) structure of the basin that will then be used as starting model for the waveform inversion. This is the first time that FATT and FWI are applied to streamer data in the Porcupine Basin. Hence, the results from this study will provide information of the velocity structure of the basin with unprecedented detail.

2 Seismic data

The seismic data set considered in this study is part of the regional multichannel seismic survey conducted in 2013-2014 over the Irish Atlantic margin by the Department of Communications, Climate Actions & Environment of Ireland together with ENI Ireland BV. Seismic data were acquired using a 10,050-m-long streamer with 804 channels and a hydrophone interval of 12.5 m. Streamer depth was 10 m, while the source was towed at 8 m depth and fired every 25 m. The field data (i.e. shot gathers) used in this study were acquired along a ~290 km long EW profile across the North Porcupine Basin (Fig. 1a). Since our study focuses on the sedimentary infill of the basin, we only use the data of a 130-km-long subsection in the central region of the line (red line in Fig. 1a)

3 Traveltime tomography of streamer data

3.1 Method

The first approximation of the V_p structure of the basin is obtained by traveltime tomography of refracted first arrivals. After a broad bandpass filtering to remove swell noise, first arrivals are clearly visible in most shot gathers (Fig. 2). Downward continuation is not applied in this case since water depths are < 600 m deep, and P-wave refracted first arrivals span from 2 to 10 km of offset in most shot gathers, which ensures a good coverage of the shallow sedimentary structure. Traveltimes of first arrivals are picked using automatic and semi-automatic approaches. The automatic approach is based on skewness and kurtosis, both commonly applied in seismology for the automatic detection of P-wave arrival times (e.g. [Saragiotis et al., 2002](#); [Hibert et al., 2013](#)). This approach samples the seismic trace using a sliding time window and computes a kurtosis value for each window (eq. 7 in [Saragiotis et al., 2002](#)). The kurtosis value is a measure of the symmetry of a distribution of a given variable with respect to the normal distribution. Hence, kurtosis values of a seismic trace are sensitive to abrupt variations in amplitude (i.e. first arrivals) (Fig. 2c). In this study, we have adapted this methodology to streamer data, which required enhancing the signal of the first arrival to make the automatic picker more effective. Hence, a broad bandpass filter (3 to 100 Hz) followed by a convolution with a user-defined filter derived from the direct wave are applied to the data. This latter step allows to significantly decrease the amount of incoherent noise (Fig. 2b). However, noisy traces can remain after this processing and hamper the automatic selection of first arrivals. To overcome this issue, we have manually picked several shot gathers along the line to create a set of *benchmark* traveltime curves for different sections of the line. The automatic detection of the first arrivals is then restricted within these benchmark models. Finally, the picking is performed manually for those shot gathers in which the signal-to-noise ratio of first arrivals was not good enough to be detected by the automatic picker. The consistency of first arrival times between successive shot gathers enabled to use the same traveltime curves for 20 consecutive shot gathers. Picking uncertainty is set between 10 and 30 ms using the method from [Zelt and Forsyth \(1994\)](#).

In order to reduce computational costs, we decimate the data by using traveltimes from only one shot gather out of four. This results in a source spacing of 100 m, which corresponds approximately to the size of the first Fresnel zone at the seafloor (at ~500 m depth), considering a dominant frequency of 40 Hz. As a result, we do not expect this decimation to decrease dramatically the resolution of the results. To ensure data redundancy, no decimation is applied to receiver sampling (12.5 m). Thus, the final data set consists of 792,097 traveltimes of first arrivals.

The velocity model is parametrized on a regular grid with 50 m node spacing both vertically and horizontally. The initial model (Fig. 1b) results from the interval velocities derived from RMS

velocities provided with the data using Dix equation (Dix, 1955) and from previous tomographic models (Prada et al., 2017). We use *TOMO2D* software (Korenaga et al., 2000) adapted to streamer data (Begovic et al., 2017) to invert for V_p . This tomographic tool uses ray theory to compute synthetic traveltimes, and a sparse matrix solver LSQR to solve the inverse problem and update the velocity model (Korenaga et al., 2000). This process is performed iteratively until residual traveltimes between observed and synthetics are minimized. Regularization parameters are defined as a set of horizontal and vertical correlation lengths that vary from top to bottom. We followed a hierarchical strategy following a three-step inversion, in which correlation lengths are decreased at each step, and the final model is used as starting model for the following step. This strategy enables to reconstruct small-scale (500-200 m wide) velocity structures through a sequential and stable process that prevents the inversion to be trapped in local minima. The final velocity model in Fig. 1b shows a good convergence with RMS residual traveltimes of ~ 20 ms, which is of the order of the picking uncertainty.

3.2 Preliminary results

The final tomographic model shows the V_p structure of the Porcupine Basin up to 4 km of depth (Fig. 1b). The sedimentary basin ranges between 95 and 180 km of profile distance with V_p of 1.5 km/s at the top and ~ 4.5 km/s at the bottom. The margins of the basins show a comparatively faster V_p transition between 3 km/s to > 5 km/s, indicating the sediment-basement transition (Fig. 1b). At the margins, the basement displays V_p of 5 and 6 km/s in agreement with previous tomographic studies in the area (Prada et al., 2017). Interestingly, the tomographic model shows several vertical low velocity anomalies at the western edge of the basin (i.e. 95-100 km of profile distance in Fig. 1b). A major anomaly is observed at 97-98 km along the line and reaching deep up to 2.5-3 km of depth, whereas a smaller anomaly is observed westwards from towards the margin and only reaching 1.5 km of depth (Fig. 1c).

To assess whether these anomalies are explained by the data or by tomographic artifacts we perform the following synthetic test: we consider a target model consisting of two prominent 1 km-wide vertical velocity anomalies (20% of the background velocity) horizontally separated 1 km away from each other (Fig. 3a). We compute synthetic traveltimes in this target model, and invert them using the background model as starting model (Fig. 3b). The result (Fig. 3c) shows that the tomographic method is able to retrieve the absolute value of both synthetic anomalies between 0.2 and ~ 2 km below seafloor (i.e. between 0.7 and ~ 2.5 km depth), which is the region where both anomalies are observed in the real tomographic model in Fig. 1b. This result confirms that this region is well constrained by the data and that the recovered 1-km-wide velocity anomalies are geologically meaningful in the final tomographic model. A first comparison of the tomographic model with the pre-stack time-migrated seismic reflection line, derived from the shot gathers used in this study (Fig. 5a), reveals that these anomalies fall on top of a major basin-bounding fault zone (Fig. 5a).

4 Waveform inversion

4.1 Method

Our waveform inversions are based on the *seisDD* package (Yuan et al., 2015, 2016), which we have adapted to large streamer datasets. This package makes use of the spectral element method *Specfem2D* (Komatitsch and Villotte, 1998) to model the full wavefield in 2D heterogeneous media. Our spectral element grid contains 250,000 elements with a typical size of 50 to 75 m. In this preliminary study, we restrict ourselves to the acoustic approximation and to the reconstruction of V_p . A density model is derived from the FATT V_p model using Gardner's law (Gardner et al., 1974) and kept fixed throughout the inversion.

The inversion process is based on the minimization of the difference between the envelopes of observed and synthetic data, via an L2-norm misfit function. Considering envelopes rather than waveforms is expected to mitigate the usual cycle-skipping issue during the first stage of the inversion. We make use of the adjoint-state method in order to compute the gradient of the misfit function efficiently, at the cost of three forward simulations per source (Tromp et al., 2008). Regularization is applied by smoothing the gradient using horizontal and vertical correlation lengths of 100 m. The local optimization is based on the quasi-Newton L-BFGS method (Nocedal and Wright, 2006).

Before comparing synthetic and observed data, we apply them the following preprocessing steps:

Low bandpass filtering: a spectral analysis of the signal-over-noise ratio indicates that data are dominated by swell noise below 5 Hz. Therefore, we apply a bandpass filter between 5 and 9 Hz to remove this low-frequency noise, as well as to start at the lowest possible frequency to mitigate cycle skipping (Sirgue and Pratt, 2004).

Mute and data selection: always in the view of mitigating the cycle skipping issue, it is important to first consider data providing wide illumination angles of the subsurface targets (Sirgue and Pratt, 2004). Therefore, in this early inversion stage, we select the long-offset refracted arrivals based on the picking of the first arrivals and on the theoretical arrival times of the direct wave propagating in the water column.

Source estimation: an accurate comparison of synthetic and observed waveforms requires the estimation of the source signature. We estimate this source wavelet in the frequency domain (Pratt, 1999) by linear inversion of the direct wave propagating in the water column, isolated from data acquired in deep water (e.g. line PAD3 in Fig. 1a).

3D-to-2D conversion: finally, we transform the observed data, acquired in the real 3D world, before comparing them to the synthetics computed in 2D, using Bleistein (1986, eq. 21).

As for the traveltimes tomography, we decimate the dataset by using one out of four shot gathers that is 1248 sources. We have verified that this decimation does not have a significant effect on the smoothed gradient used for the optimization.

4.2 Preliminary results

4.2.1 Forward modelling: comparison of synthetics with observed data

Figure 4 presents a comparison of observed and synthetic data computed in the initial interval velocity model derived from RMS velocities (Fig. 1a) and in the final FATT model (Fig. 2b), for a source located at 90 km along the profile, which corresponds to a shot gather spanning over the fault zone shown in Fig. 5. Observed and synthetic shot gathers are presenting in a symmetric way, such as to facilitate the comparison of the refracted arrivals at far offset. Synthetic data computed in the final FATT model clearly match the observations much better than in the initial velocity model, not only for the first arrivals fitted by the traveltimes tomography, but also for later arrivals. This confirms that the final FATT velocity model is a much better starting model for FWI.

4.2.2 Towards inversion: preliminary V_p gradient

Figure 5b shows the preliminary V_p gradient obtained by correlating, time integrating and summing forward and adjoint wavefields from all the 1248 considered sources. This image can be understood as the perturbation that needs to be added to the starting model (final FATT model) in order to better fit the data. The gradient on the western margin of the basin reveals interesting features in the fault zone already identified in the FATT model (Fig. 5a). In particular, the alternation of slow and fast pseudo-vertical velocity structures is very consistent with the FATT model and correlate well with the presence of faults on the migrated section (Fig. 5b). Even though we did not update the starting model yet, we consider this preliminary result as very promising in view of the inversion.

5 Future work

Future work on FATT will focus on the integration of well data and on the assessment of porosity variations across the fault zone to interrogate the geological meaning of these anomalies. In addition, we will perform a Monte Carlo analysis and a Checkerboard test to evaluate the sensitivity of the final tomographic model to the starting model, and the lateral resolution of our results, respectively.

Regarding FWI, once a first model is obtained further work will focus on multiparameter FWI, first in the acoustic approximation for the joint estimation of V_p and density, and second considering elastic wave propagation for further estimation of V_s , and eventually of attenuation and anisotropy. These additional parameters are expected to provide valuable information on subsurface petrophysical properties. In particular, density and V_p/V_s ratios could be interpreted in terms of porosity, fluid content, and lithology.

Acknowledgments

This publication has emanated from research supported in part by a research grant from Science Foundation Ireland (SFI) under Grant Number 13/RC/2092 and is co-funded under the European Regional Development Fund and by PIPCO RSG and its member companies. Seismic data were provided by the Petroleum Affairs Division of the Department of Communications, Climate Action and Environment, Ireland. The authors wish to acknowledge the DJEI/DES/SFI/HEA Irish Centre for High-End Computing (ICHEC) for the provision of computational facilities and support. Generic Mapping Tools (Wessel and Smith, 1995) and Seismic Unix software package (Stockwell, 1999) were used in the preparation of this manuscript.

References

- Amante, C. & Eakins, B.W., (2009). ETOPO1 1 Arc-Minute Global Relief Model: Procedures, Data Sources and Analysis. NOAA Technical Memorandum NESDIS NGDC-24. National Geophysical Data Center, NOAA. doi:10.7289/V5C8276M.
- Begović, S., A. Meléndez, C. Ranero, & V. Sallarès (2017) Joint refraction and reflection travel-time tomography of multichannel and wide-angle seismic data. EGU General Assembly 2017, Vienna, Austria, Poster EGU2017-17231
- Bleistein, N. (1986). Two-and-one-half dimensional in-plane wave propagation. *Geophysical Prospecting*, 34:686-703.
- Červený, V. (2001). *Seismic Ray Theory*. Cambridge University Press, Cambridge.
- Delescluse, M., Nedimović, M. R., & Louden, K. E. (2011). 2D waveform tomography applied to long-streamer MCS data from the Scotian Slope. *Geophysics*, 76(4):B151-B163.
- Dix, C. H. (1955). Seismic Velocities from Surface Measurements, *Geophysics* 20, no. 1: 68–86.

- Enachescu, M. E. & Hogg, J. R. (2005). Exploring for Atlantic Canada's next giant petroleum discovery. *CSEG Recorder*, 30(5), 19-30.
- Erickson, S. N. & Jarrard, R. D. (1998). Velocity-porosity relationships for water-saturated siliciclastic sediments. *Journal of Geophysical Research: Solid Earth*, 103(B12), 30385-30406.
- Gardner, G., Gardner, L., & Gregory, A. (1974). Formation velocity and density — the diagnostic basics for stratigraphic traps. *Geophysics*, 39(6):770-780.
- Hovland, M., Croker, P. F., & Martin, M. (1994). Fault-associated seabed mounds (carbonate knolls?) off western Ireland and north-west Australia. *Marine and Petroleum Geology*, 11(2), 232-246.
- Komatitsch, D. & Vilotte, J. P. (1998). The spectral element method: an efficient tool to simulate the seismic response of 2D and 3D geological structures. *Bulletin of the Seismological Society of America*, 88:368-392.
- Korenaga, J., Holbrook, W. S., Kent, G. M., Kelemen, P. B., Detrick, R. S., Larsen, H. C., Hopper, J. R. & Dahl-Jensen, T. (2000). Crustal structure of the southeast Greenland margin from joint refraction and reflection seismic tomography. *Journal of Geophysical Research - Solid Earth*, 105, 21591-21614, doi:10.1029/2000JB900188.
- Naeth, J., Primio, R., Horsfield, B., Schaefer, R. G., Shannon, P. M., Bailey, W. R., & Henriot, J. P. (2005). Hydrocarbon seepage and carbonate mound formation: a basin modelling study from the Porcupine Basin (offshore Ireland). *Journal of Petroleum Geology*, 28(2), 147-166.
- Nocedal, J. & Wright, S. J. (2006). *Numerical Optimization*. Springer, 2nd edition.
- Pratt, R. G. (1999). Seismic waveform inversion in the frequency domain, Part 1: Theory and verification in a physical scale model. *Geophysics*, 64(3):888-901.
- Prada, M., Watremez, L., Chen, C., O'Reilly, B. M., Minshull, T. A., Reston, T.J., Shannon, P.M., Klaeschen, D., Wagner, G. & Gaw, V. (2017), Crustal strain-dependent serpentinisation in the Porcupine Basin, offshore Ireland, *Earth and Planetary Science Letters*, 474, 148-159, doi:10.1016/j.epsl.2017.06.040
- Sarigiotis, C. D., Hadjileontiadis, L. J., & Panas, S. M. (2002). PAI-S/K: A robust automatic seismic P phase arrival identification scheme. *IEEE Transactions on Geoscience and Remote Sensing*, 40(6), 1395-1404.
- Shannon, P. M., Moore, J. G., Jacob, A. W. B., & Makris, J. (1993). Cretaceous and Tertiary basin development west of Ireland. In *Geological Society, London, Petroleum Geology Conference series* (Vol. 4, No. 1, pp. 1057-1066). Geological Society of London.
- Sirgue, L., & Pratt, R. G. (2004). Efficient waveform inversion and imaging: A strategy for selecting temporal frequencies. *Geophysics*, 69(1), 231-248.
- Srivastava, S. P., & Verhoef, J. (1992). Evolution of Mesozoic sedimentary basins around the North Central Atlantic: a preliminary plate kinematic solution. *Geological Society, London, Special Publications*, 62(1), 397-420.
- Stockwell, J. W. (1999), The CWP/SU: Seismic unix package, *Computers & Geosciences*, 25(4), 415–419.
- Tromp, J., Komatitsch, D., & Liu, Q. (2008). Spectral-element and adjoint methods in seismology. *Communications in Computational Physics*, 3(1):1–32.
- Virieux, J. & Operto, S. (2009). An overview of full-waveform inversion in exploration geophysics. *Geophysics*, 74(6):WCC127–WCC152.
- Wessel, P. & Smith, W. H. (1998). New, improved version of Generic Mapping Tools released. *Eos, Transactions American Geophysical Union*, 79, 579-579, doi:10.1029/98EO00426
- Worthington, R. P., & Walsh, J. J. (2016). Timing, growth and structure of a reactivated basin-bounding fault. *Geological Society, London, Special Publications*, 439, SP439-14.
- Y. O. Yuan, F. J. Simons, & E. Bozdağ. Multiscale adjoint waveform tomography for surface and body waves. *Geophysics*, 80(5):R281-R302, 2015.

Yuan, Y. O., Simons, F. J., & Tromp, J. (2016). Double-difference adjoint seismic tomography. *Geophysical Journal International*, 206(3):1599-1618.

Zelt, C. A., & Forsyth, D. A. (1994). Modeling wide-angle seismic data for crustal structure: Southeastern Grenville Province. *Journal of Geophysical Research - Solid Earth*, 99, 11687-11704, doi:10.1029/93JB02764.

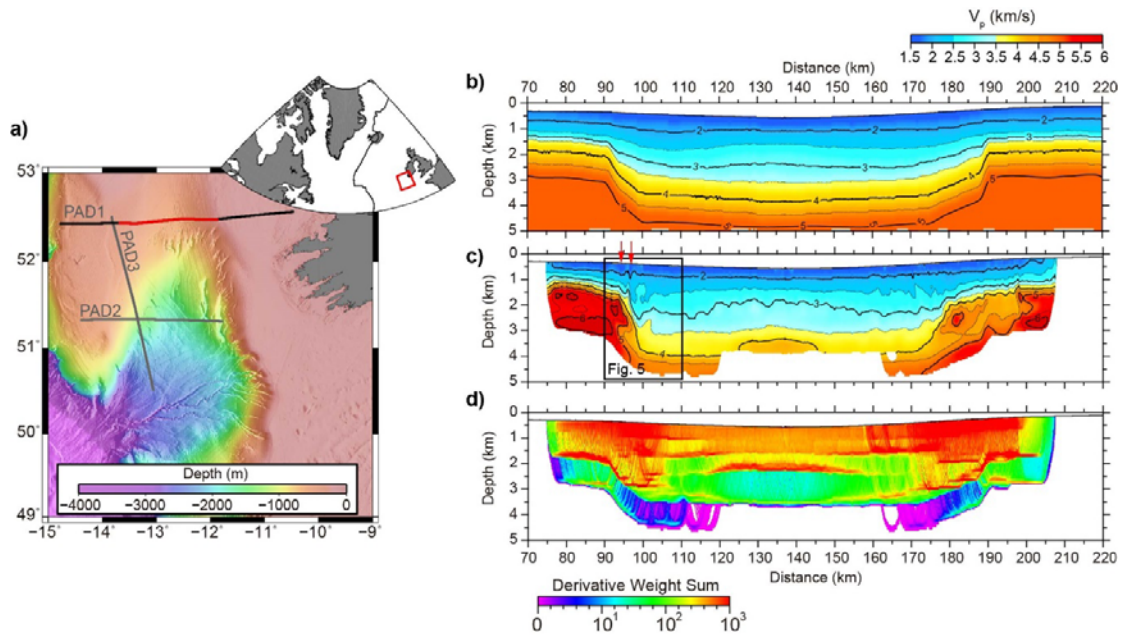


Figure 1. (a) Bathymetry map of the Porcupine Basin located SW of Ireland (see inset). The red line shows the section of PAD 1 (black line) used to apply FATT and FWI in this study. Grey lines will be used in future studies. Bathymetry data set is extracted from [Amante and Ekins \(2009\)](#). (b) Starting V_p model from RMS velocities. (c) Final FATT model showing the velocity structure resolved by the inversion. Red arrows show the location of both low velocity anomalies discussed in section 3.2. Black box contains the region enlarged in Fig. 5. (d) Derivative weight sum of the final tomographic model, which is a proxy of the ray coverage through the model.

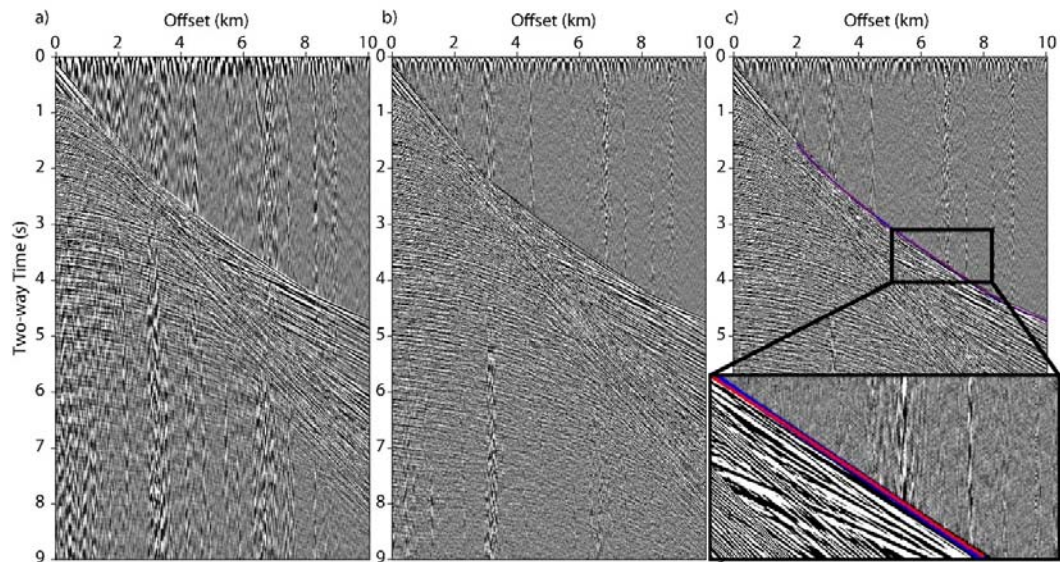


Figure 2. (a) Shot gather along line PAD1 filtered using a bandpass filter (3-100 Hz), and (b) convolved with a user-defined filter derived from the direct wave. (c) Same shot gather showing the automatically picked traveltimes (in blue) and synthetic traveltimes after the inversion (in red).

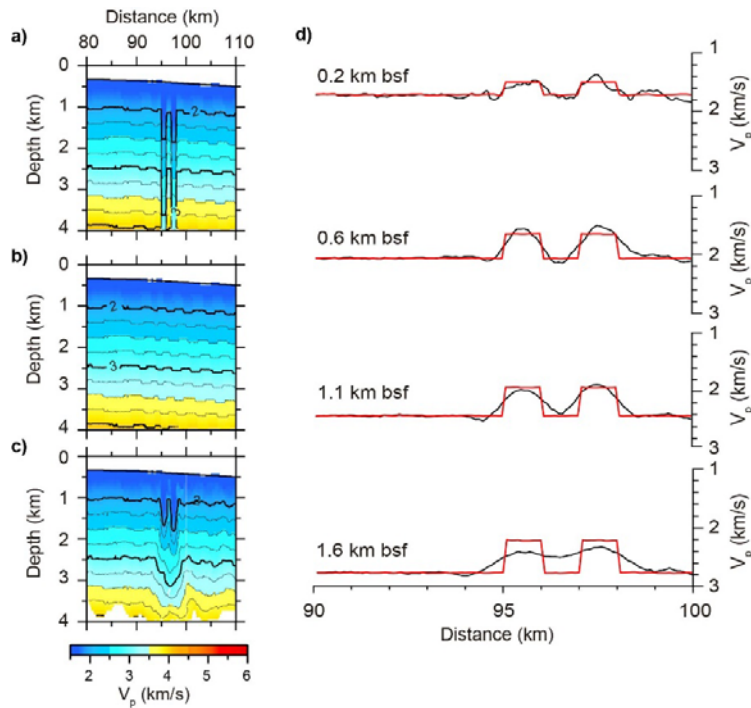


Figure 3.- (a-c) Synthetic test showing the retrieval of two 1-km-wide anomalies. (a) Target model, (b) starting model, and (c) final model (see section 3.2 for details on the analysis) (d) Horizontal 1D V_p profiles extracted across both anomalies at different depths below seafloor (bsf).

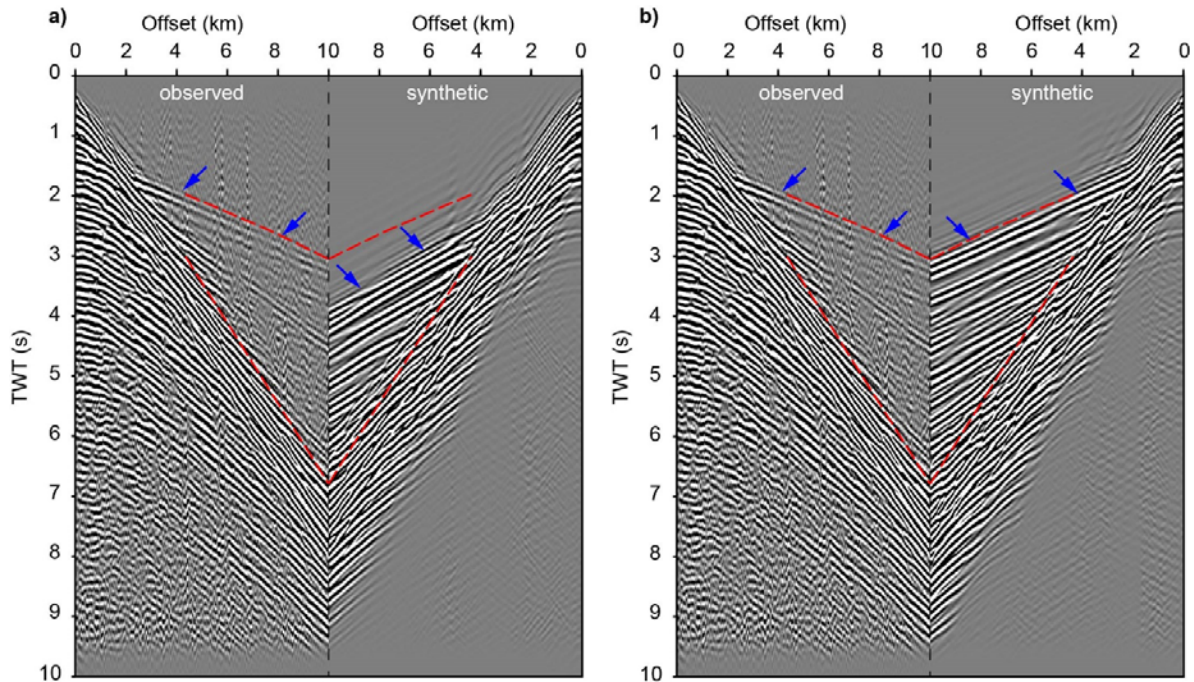


Figure 4.- Comparison of observed data with synthetics computed (a) in the initial velocity model (Fig. 1b) and (b) in the final FATT V_p model (Fig. 1c), for a shot gather spanning over the basin-bounding fault zone of Fig. 5 (source located at 90 km). The red dashed lines indicate the mute window applied for data selection in view of the inversion. Blue arrows depict the location of first arrivals in the sections.

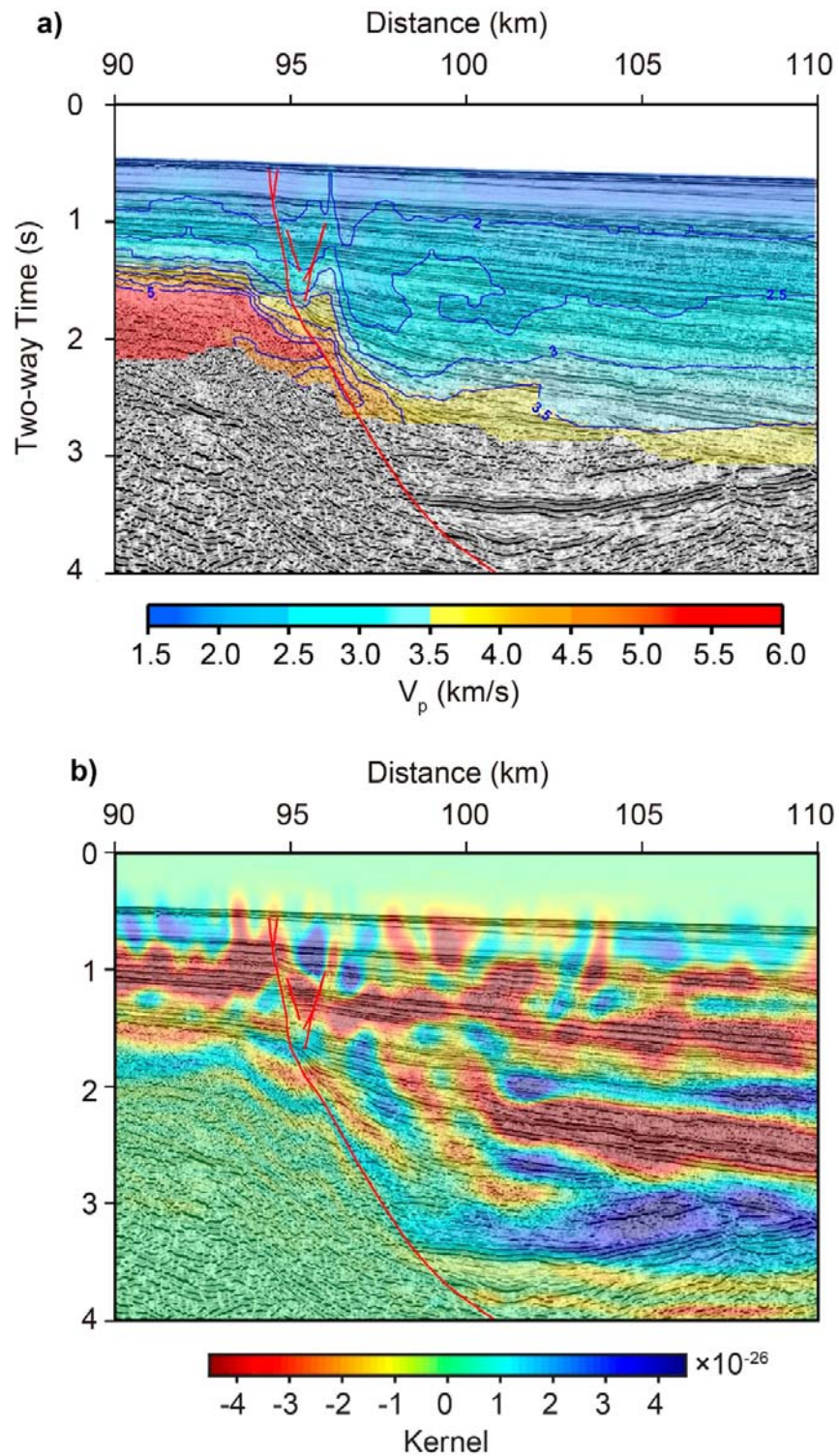


Figure 5. Close up of the FATT V_p model in Fig. 1c overlaying the pre-stack time-migrated section at the western margin of the basin after depth-to-time conversion. Blue lines are iso-velocity contours from the FATT V_p model (in km/s). Note that red lines show a major basin-bounding fault zone that coincides with a low velocity anomaly. **(b)** Preliminary FWI V_p gradient overlaying the same pre-stack time-migrated section as in **(a)**. Negative (red) values indicate areas where the inversion may introduce faster velocity zones, while positive (blue) gradient values indicate slower velocities.